Generalized Integrator-Extended State Observer With Applications to Grid-Connected Converters in the Presence of Disturbances

Baoling Guo, Seddik Bacha, Mazen Alamir, Ahmad Hably, Cédric Boudinet

Generalized Integrator-Extended State Observer with Applications to Grid-connected Converters in Presence of Disturbances

Baoling Guo, Seddik Bacha, *Senior member, IEEE,* Mazen Alamir, *Member, IEEE,* Ahmad Hably, *Member, IEEE,* Cédric Boudinet

***Abstract*—Large-scale Fast-Varying Sinusoidal Disturbances (FVSD) impact strongly the operation of Grid-connected Converters (GcCs). A conventional Extended State Observer (ESO) is not sufficiently capable to deal with these rapid disturbances. This critical weakness has limited ESO's applications to GcCs. Therefore, a Generalized Integrator-ESO (GI-ESO) is developed from ESO to address such issues. Knowing that grid common disturbances can be expressed as a phase, frequency, or magnitude disturbed sinusoidal signal. Multi-GIs of selective resonant frequencies are hence applied into the disturbance estimation loop, which enables FVSD to be observed with a relatively low bandwidth. Besides, a frequency-adaptive mechanism is introduced in order to mitigate the effects of frequency deviations. The proposed GI-ESO resolves the trade-off between the observer's bandwidth and the noise filtering. A case of three-phase phase-locked loop control system of disturbed regimes is in particular studied to assess the performance of GI-ESO and the stability of resulting controlled system. Theoretical analysis and experimental results have proven its effectiveness in applications to GcCs in presence of various disturbances.**

***Index Terms*—Grid-connected converters, Extended State Observer, generalized integrator, fast-varying sinusoidal disturbances, phase-locked loop, frequency-adaptive mechanism.**

I. Introduction

DISTURBANCES and uncertainties present in the control systems require the design of robust controllers [1]–[5]. Thus, various robust approaches based on disturbance rejection have been proposed such as unknown input observer [1], disturbance observer [2], and Extended State Observer (ESO) [3]–[5], etc. However, the performance of model-based observers and its resulting control systems are sensitive to model parameters deviations [2]. ESO has been widely used as a partial-model-based observer, being less dependent on the knowledge of the system [3]–[8]. ESO is proposed in the frame of Active Disturbance Rejection Control (ADRC), which can also work independently with other controllers [6]. ESO has been originally proposed with a nonlinear structure [3], while the linear ESO has been broadly employed as it is easier to design and to implement for practitioners [4].

This work is supported by PSPC Innov'hydro project, which brings together General Electric (GE) Renewable Energy, eDF (Électricité de France), Grenoble INP, and other key players in the hydroelectric sector, in France.

B. Guo, the corresponding author, is with the University Grenoble Alpes, CNRS, Grenoble INP*, G2Elab, F-38000, Grenoble, France (email: baoling.guo@g2elab.grenoble-inp.fr).

S. Bacha and C. Boudinet are with the University Grenoble Alpes, CNRS, Grenoble INP*, G2Elab, F-38000, Grenoble, France (email: seddik.bacha@g2elab.grenoble-inp.fr; cedric.boudinet@g2elab.grenoble-inp.fr).

M. Alamir and A. Hably are with the University Grenoble Alpes, CNRS, Grenoble INP*, GIPSA-Lab, F-38400, Saint Martin D'Hères, France (email: mazen.alamir@gipsa-lab.grenoble-inp.fr; ahmad.hably@gipsa-lab.grenoble-inp.fr).

* Institute of Engineering Univ. Grenoble Alpes

The performances of ADRC- or ESO- based controllers primarily depend upon the accuracy of the state and disturbances estimation [3]. Large efforts have been devoted to the tracking error convergence analysis of nonlinear or linear ESOs [9]–[12]. The authors of [9], [10] have respectively proven that ESO can achieve the asymptotic convergence for constant disturbances. In another work [11], it has been shown that the ESO estimation error remains bounded if the changing rate of time-varying uncertainties is bounded. Theoretically, the estimation precision of ESO for time-varying disturbances can be improved by increasing its bandwidth. However, the bandwidth is limited by the presence of sensor noises and dynamic uncertainties, otherwise large high-frequency noises from the output side would be transferred to the control signal [13]. Many attempts have been made to deal with a class of time-varying disturbances in [14]–[18]. A Proportional Integral Generalized (GPI) observer-based control approach has been discussed in [15], [16], which is actually in line with the Generalized ESO (GESO) presented in [14]. A spatial observer-based repetitive controller is then proposed for mechatronic systems in [17], which is developed from the GPI approach described in [15], [16]. It has been proven that if the rth-order derivative of disturbance becomes zero, the asymptotic convergence for its state estimate can be achieved by employing rth-order GESO or GPI in [14]–[16]. However, a sinusoid is a type of infinitely differentiable disturbances [14]. The performance of higher-order ESO in tracking sinusoidal disturbances has been analysed in [12]. It has been shown that a higher-order GESO offers better estimation accuracy in comparison with a conventional ESO, provided that the observer bandwidth is chosen sufficiently larger than the frequency of the disturbance. Consequently, the higher-order GESO or GPI can only ensure the precision for limitedly low-frequency sinusoidal disturbances. The GESO/GPI is not sufficiently capable to deal with very Fast-Varying Sinusoidal Disturbances (FVSD) such as harmonics-related disturbances that are multiples of grid fundamental frequency. Moreover, the authors of [18] propose a proportional integral observer in order to mitigate the effects of high-frequency measurement noises or modeling errors, however, the performance regarding FVSD are not dedicatedly discussed.

Grid-connected Converters (GcCs) have various types of industrial applications such as grid-integrated renewable energy generation systems [19], micro-grid systems [20], uninterruptible power supplies [21], etc. In practice, various disturbed regimes have to be taken into account regarding the control design of GcCs. Firstly, transient voltage sags and long-term voltage unbalances commonly happen in power systems [22], the unbalanced voltages then cause second-

order harmonics to appear in the control systems. Besides, the power-electronics devices and industrial nonlinear loads are largely penetrated into the power grid, which induce large harmonics in the control system of GcCs [19], [23]. The voltage offset introduced by the offset of signal measurements or conversion circuits can not be neglected as well [24]. Also, the power fluctuations can lead to grid frequency deviations from the nominal value (50Hz or 60Hz) [25]. Note that the grid frequency deviations are limited by international standards [25], [26]. Key features of the disturbances present in GcCs are summarized as follow: 1) They are very fast-varying sinusoidal disturbances; 2) Their frequencies are roughly known, being positive integer multiples of grid fundamental frequency.

Regarding the conventional ESO or the higher-order GESO, neither of them can efficiently identify such FVSD. Then, the performances of resulting GcCs control systems would be seriously affected. Take a three-phase Phase-Locked Loop (PLL) control system for example, it is commonly employed to achieve the grid synchronization for GcCs [24], [27]. The ESO-based PLL can achieve satisfying performance if no harmonics pollute the control system [28]. In practice, grid voltages are not pure balanced sinusoids but disturbed by unbalances, harmonics, and voltage offsets [19], [22]–[24]. The harmonics components then appear in the estimated output phase angle. Finally, the control performance of GcCs is degraded due to the bad quality output of a PLL. In addition, the SRF-PLLs are commonly equipped with additional filters under disturbed regimes [28], such as Decoupled PLL (DPLL) [29] and Moving Average Filter PLL (MAF-PLL) [30]. The DPLL can deal with the unbalanced grid perfectly, and the results for harmonics polluted grids are practically accepted but not satisfactory [29]. The MAF-PLL, however, presents a slow dynamic response [30]. More critically, neither of them can effectively deal with the voltage offset. A Generalized Integrator-Extended State Observer (GI-ESO) is thus proposed in this work, which then can be employed to address such issues for its applications into grid-connected converters.

Generalized Integrator (GI), also known as resonant controller, has been widely used for different purposes [19], [23], [31], [32]. In this work, a GI-ESO is developed from the conventional ESO. The pure integrator is maintained to track Direct Current (DC)-type or very low-frequency disturbances. Besides, GIs of different resonant frequencies are inserted into the disturbance estimation loop to deal with the FVSD. Furthermore, a frequency-adaptive mechanism is introduced in order to mitigate the effects of frequency deviations. This design enables FVSD to be observed with a relatively low bandwidth, which resolves the trade-off between the bandwidth of ESO and the high-frequency noises filtering. A three-phase PLL control system under disturbed regimes is chosen as an example to assess the effectiveness of the proposed GI-ESO and the stability of resulting control system.

The paper is organized as follows: the problem formulation is described in Section II, a case of three-phase PLL system is in particular chosen as an example to formulate the control issues. The proposed GI-ESO is designed and then applied to the three-phase PLL system in Section III, meanwhile, the control stabilities and the tuning guidelines are discussed in details. Then, experimental results under various disturbed regimes are provided to assess its effectiveness in Section IV. Concluding remarks are provided in Section V.

II. Problem Formulation

A disturbed GcC with its commonly used control structure is illustrated in Fig. 1. The control of GcCs primarily has three functions: the grid synchronization [28], the grid current control [19], and the DC-link voltage control [33]. As aforementioned in Section I, large sinusoidal disturbances could be present in the control system of GcCs under disturbed regimes. These disturbances show the following common features:

1) They are very fast-varying sinusoidal disturbances;
2) Their frequencies are roughly known, being positive integer multiples of the grid fundamental frequency.

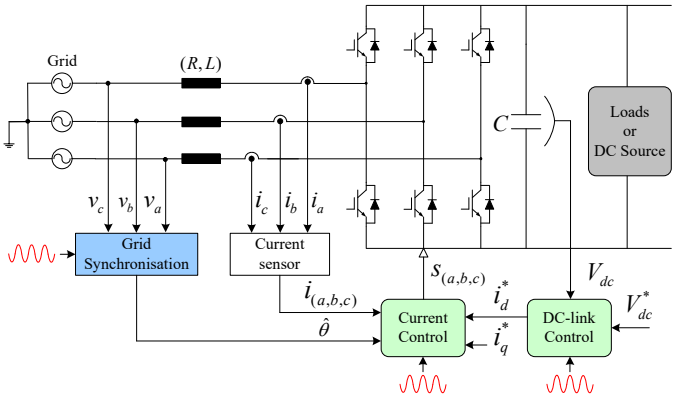

Fig. 1: Schematic diagram of a disturbed grid-connected converter with the commonly used control structure, with $i_{(abc)}$ the grid currents, $v_{(abc)}$ the grid voltages, i_d^* and i_q^* the d-axis and the q-axis grid current references, V_{dc} the DC-link voltage, C the DC-link capacitance, L and R the filter inductance and resistance, respectively, $S_{(a,b,c)}$ the switching states.

The proper synchronization with grid voltage is important to ensure the whole performances of resulting GcCs control systems. In this work, the case of Synchronous Reference Frame Phase-Locked Loop (SRF-PLL) is chosen as an illustrative example to formulate the control issues and then to assess the effectiveness of the proposed GI-ESO.

A. SRF-PLL modeling and error analysis

A common design diagram of SRF-PLL is described in Fig. 2(a), which is composed of a Phase Detector (PD), a Loop Filter (LF), and a Voltage-Controlled Oscillator (VCO) [27]. More design details can be found in [24], [27], [28], but some key aspects are worth to be highlighted:

- The magnitude V_m acts as a gain in the forward path of the linear model as illustrated in Fig. 2(b). This means that the magnitude variations can affect the loop gain and, therefore, the stability margins and dynamic behaviour of SRF-PLL. That is the reason why, a magnitude normalization scheme is usually introduced in order to decouple the effects from magnitude variations [27].

- Two saturation blocks are also introduced: the saturation block of d-axis voltage is used to avoid the division by zero in the transient process; the saturation block of the controller is used to ensure that the estimated frequency meets the related international standards.

Note that ESO- or GI-ESO- based SRF-PLLs presented later also follow the above principles.

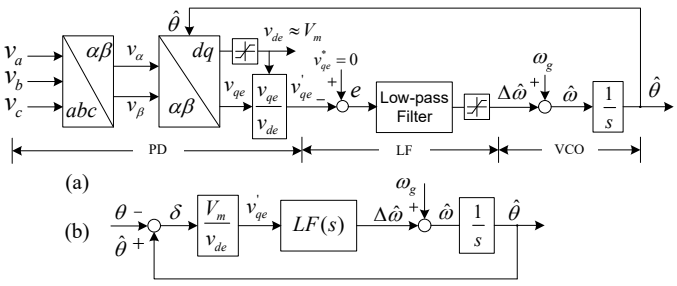

Fig. 2: (a) Schematic diagram of conventional SRF-PLL, (b) linear model, with v_{qe}, v_{de} the voltages in a dq synchronous reference frame, v_α, v_β the voltages in a $\alpha\beta$ rotating reference frame, V_m the grid voltage magnitude, ω_g the grid nominal angular frequency, $\hat{\omega}$ the estimated angular frequency, $\Delta\hat{\omega}$ the estimated angular frequency deviation, $\hat{\theta}$ the estimated phase angle, and $LF(s)$ is the transfer function of LF

The modeling and estimation errors analysis of SRF-PLL for various disturbed regimes have been proposed in [24]. The unbalanced case is in particular presented in this section. The errors analysis of SRF-PLL in presence of harmonics and voltage offsets are provided in Appendix A. The unbalanced voltages can be represented by:

$$\begin{bmatrix} v_a \\ v_b \\ v_c \end{bmatrix} = V_m \begin{bmatrix} \cos\theta \\ (1+A)\cos(\theta - \frac{2\pi}{3}) \\ (1+B)\cos(\theta + \frac{2\pi}{3}) \end{bmatrix} \tag{1}$$

where A and B represent the unbalanced levels. With Park transform [24], the q-axis voltage is given by:

$$\begin{aligned} v_{qe} = V_m \sin\delta - V_m \Big[&\frac{A-B}{2\sqrt{3}} (\cos\theta\cos\hat{\theta} - \sin\theta\sin\hat{\theta}) \\ &+ \frac{A+B}{6} (\sin\theta\cos\hat{\theta} + \cos\theta\sin\hat{\theta}) \Big] \end{aligned} \tag{2}$$

The phase error $\delta = \hat{\theta} - \theta$ is very small ($\theta \approx \hat{\theta}$), and the $\theta + \hat{\theta} \approx 2\theta$, the expression can be rewritten by

$$v_{qe} \approx V_m \big[\delta - E_{2\omega} \cos(2\theta + \phi_{ub})\big] \tag{3}$$

where

$$E_{2\omega} = \sqrt{\Big(\frac{A-B}{2\sqrt{3}}\Big)^2 + \Big(\frac{A+B}{6}\Big)^2}$$

$$\phi_{ub} = -\tan^{-1}\Big(\frac{1}{\sqrt{3}}\frac{A+B}{A-B}\Big).$$

Under an unbalanced grid condition, the sinusoidal disturbances would be transmitted to the output phase angle [24]. The phase error caused by the voltage unbalances can be expressed as follows:

$$0 < |\delta| \leq E_{2\omega} |\cos(2\theta + \phi_{ub})| \tag{4}$$

B. ESO-based SRF-PLL design principles and its limitations

An ESO-based controller is used in order to enhance control dynamics of SRF-PLLs in [28]. First, the design principles are briefly reviewed. Then, the ESO's limitations when used in disturbed grids are analyzed and experimentally revealed.

The control diagram of the ESO-based SRF-PLL is shown in Fig. 3, where an ESO-based corrector is used as the LF. ESO is used to track the unknown disturbances in the PLL system. The estimated disturbances $\hat{x}_2$ are actively compensated into the signal u_0 in real-time.

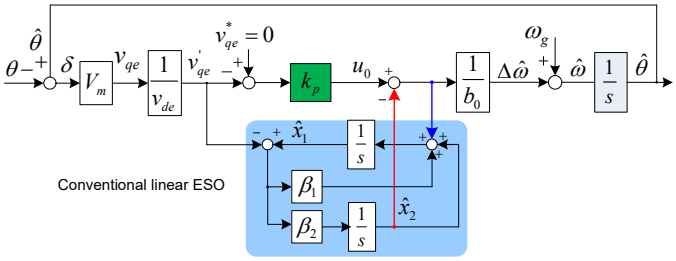

Fig. 3: Conventional ESO-based SRF-PLL control diagram, $\hat{x}_1$ is the estimation of $v_{qe}^{'}$, $\hat{x}_2$ is the estimation of total unknown disturbances, β_1 and β_2 are the tuned positive gains of ESO, b_0 is the estimation of control gain

The first step before using an ESO-based controller is to reformulate a practical control issue in the canonical form of cascaded integrators with generalized disturbances [8]. By differentiating and simply manipulating the expression (3), the canonical form becomes:

$$\frac{1}{V_{de}}\frac{dv_{qe}}{dt} = \frac{V_m}{V_{de}}\frac{d(\hat{\theta}-\theta)}{dt} = b_0\Delta\hat{\omega} + f \tag{5}$$

An appropriate disturbance definition is critical to achieve a high-efficiency ESO [8]. In the PLL, v_{de} stands for the real-time estimation of V_m, therefore, the control gain $b = V_m/v_{de}$ approximates 1. It is reasonable to set the estimation of control gain with $b_0 = 1$. Moreover, the nominal grid frequency ω_g is feed-forwarded in the control input. Such compensation improves ESO estimation's precision and response dynamics. Finally, the total disturbances f is formulated by:

$$\begin{aligned} f &= [(b-b_0)\Delta\hat{\omega} + (\omega_g - \omega) + d_x] + 2\omega E_{2\omega}\sin(2\theta + \phi_{ub}) \\ &= d_{(0)} + d_{(2\omega)} \end{aligned} \tag{6}$$

where $d_{(0)} = (b-b_0)\Delta\hat{\omega} + (\omega_g - \omega) + d_x$, and $(b-b_0)\Delta\hat{\omega}$ is due to the small mismatch between b and b_0, $\omega_g - \omega$ is the grid frequency variations, d_x represents extra disturbances such as low-frequency disturbances induced by phase jumps, time-varying parameters, nonlinear dynamics, etc.; $d_{(2\omega)} = 2\omega E_{2\omega}\sin(2\theta + \phi_{ub})$ represents the harmonics disturbances.

To highlight, the frequency deviations, the voltage magnitude variations, and phase jumps have a physically limited changing rate in the power system like the majority of related signals. For instance, the frequency jump is related to the speed variations of the synchronous generators which have their own inertia. For the inrush currents and voltages, the phase jump can be considered as ramps even for phenomenon with a very short interval time. In conclusion, the signals we are referring to are differentiable with bounded derivatives.

In the sequel, the following definitions are used: $\Delta\hat{\omega}$ is the control input u, v_{qe}^{*} is the reference r, $v_{qe}^{'}$ is the output y, which is defined as a state variable by $x_1 = v_{qe}^{'}$, f is treated as an extended state variable, and expressed by $x_2 = f$, its time derivative is given by $\dot{x}_2 = h$ [28]. Now, the state space model can be constructed as follows:

$$\begin{bmatrix} \dot{x_1} \\ \dot{x_2} \end{bmatrix} = \begin{bmatrix} 0 & 1 \\ 0 & 0 \end{bmatrix} \begin{bmatrix} x_1 \\ x_2 \end{bmatrix} + \begin{bmatrix} b_0 \\ 0 \end{bmatrix} u + \begin{bmatrix} 0 \\ 1 \end{bmatrix} h \tag{7}$$

Based on (7), the ESO can be formulated as follows:

$$\begin{bmatrix} \dot{\hat{x}}_1 \\ \dot{\hat{x}}_2 \end{bmatrix} = \begin{bmatrix} 0 & 1 \\ 0 & 0 \end{bmatrix} \begin{bmatrix} \hat{x}_1 \\ \hat{x}_2 \end{bmatrix} + \begin{bmatrix} b_0 \\ 0 \end{bmatrix} u + \begin{bmatrix} \beta_1 \\ \beta_2 \end{bmatrix} [x_1 - \hat{x}_1] \tag{8}$$

where $\hat{x}_1$ is the estimation of $v_{qe}^{'}$, $\hat{x}_2$ is the estimation of total disturbances, β_1 and β_2 are positive gains of ESO.

By subtracting (8) from (7), the error dynamics are defined by:

$$\begin{bmatrix} \dot{e_1} \\ \dot{e_2} \end{bmatrix} = \underbrace{\begin{bmatrix} -\beta_1 & 1 \\ -\beta_2 & 0 \end{bmatrix}}_{\mathrm{A}_e} \begin{bmatrix} e_1 \\ e_2 \end{bmatrix} + \begin{bmatrix} 0 \\ 1 \end{bmatrix} h \tag{9}$$

where $e_1 = x_1 - \hat{x}_1$ is the state estimation error, and $e_2 = x_2 - \hat{x}_2$ is the disturbances estimation error. The positive gains $\beta_1 = 2\omega_o$ and $\beta_2 = \omega_o^2$ are chosen such that the characteristic polynomial (10) is Hurwitz stable [4].

$$\lambda(s) = (sI - A_e)^{-1} = s^2 + \beta_1 s + \beta_1 2 = (s + \omega_o)^2 \tag{10}$$

where ω_o is referred to as the bandwidth of ESO [4].

Based on Fig. 3, the control law is formulated by

$$\Delta\hat{\omega} = \frac{k_p(v_{qe}^{*} - v_{qe}^{'}) - \hat{x}_2}{b_0} \tag{11}$$

If the total disturbances were correctly estimated and compensated, the original plant model would be reduced to be a pure integrator [34]. Then, the closed-loop transfer function can be approximated by

$$H_c(s) \approx \frac{k_p \frac{1}{s}}{1 + k_p \frac{1}{s}} = \frac{1}{1 + \frac{s}{k_p}} \tag{12}$$

where $\omega_c \approx k_p$ is referred to as the closed-loop bandwidth.

More details on convergence analysis, stability analysis, and tuning methods can be found in [4], [7], [34], [35].

C. ESO's limitations in tracking the FVSD

Based on (9), the transfer function of disturbances estimation error becomes:

$$f_{e_2}(s) = \frac{e_2(s)}{f(s)} = \frac{s(s + 2\omega_o)}{(s + \omega_o)^2} \tag{13}$$

The bode plots of $f_{e_2}(s)$ are shown in Fig. 4, with $\omega_o \in \{300, 400, 500\}$ (rad/s). It can be observed that ESO behaves like a low-pass filer with respect to the input disturbances [34]. The conventional ESO can estimate the unknown disturbance very well only when the disturbances are composed of low-frequency components. The estimation errors of disturbances can be reduced by increasing the bandwidth ω_0, however, the bandwidth would be limited by the practical noises.

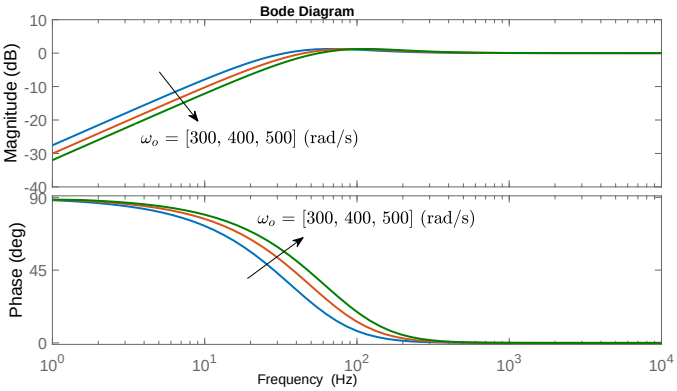

Fig. 4: Bode diagram of the transfer function $f_{e_2}(s)$

Experimental results are obtained by using the dSPACE controller (DS2005). Three-phase voltages are configured as shown in Fig. 5: at the beginning, three-phase voltages are considered to be balanced with $V_m = 100V$, $A = B = C = 0\%$; then, the unbalanced regime is set to $V_m = 100V$, $A = 0\%$, $B = 30\%$, and $C = 30\%$.

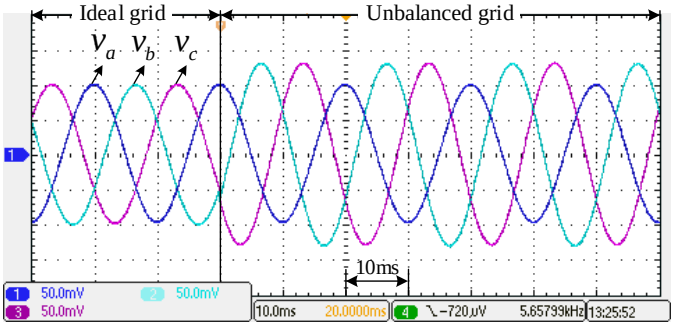

Fig. 5: Three phase voltages, v_a, v_b, v_c (50V/div)

Following the tuning rules as [28], the control parameters are configured with $\omega_c = 100$ rad/s and $\omega_o = 400$ rad/s. The results of ESO-based SRF-PLL are shown in Fig. 6. The grid phase angle is correctly estimated for the ideal grid; while the phase estimation errors are not negligible in presence of grid unbalances. The reason is that the total disturbances defined by (6) are partially filtered by ESO, the second-order harmonics are then introduced into the estimated phase angle.

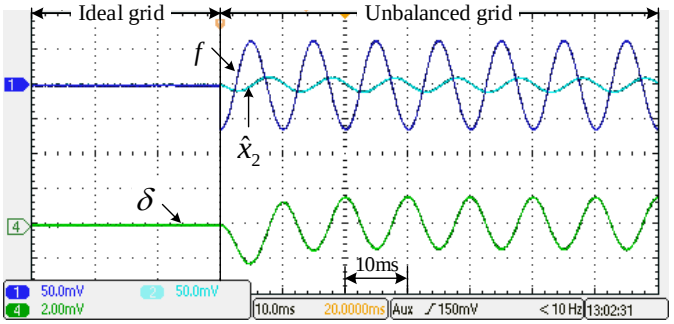

Fig. 6: Performance of conventional ESO-based SRF-PLL, f the total disturbances (50/div), $\hat{x}_2$ the estimated disturbances by ESO (50/div), δ the estimated phase error (2°/div)

The ESO-based PLL can also be equipped with additional filters under disturbed regimes such as DPLL and MAF-PLL, but neither of them can efficiently deal with the voltage offsets. A GI-ESO is therefore proposed to address such issues for its applications into grid-connected converters.

III. GI-ESO DEIGN AND ITS APPLICATION TO SRF-PLL

In this section, the main properties of GI-ESO are firstly highlighted. Then, a GI-ESO-based SRF-PLL is designed in order to assess the performance of the proposed GI-ESO and the stability of its resulting control system.

A. GI-ESO design

The GI-ESO is developed from the previous linear ESO. It inherits the ESO's original advantages: high robustness, good disturbance rejection abilities within the bandwidth of ESO, and simple tuning methods [4]. More critically, the capability in dealing with FVSD are enhanced for the proposed GI-ESO.

1) Extended structure and mathematical model

The proposed GI-ESO and the conventional ESO are comparatively presented in Fig. 7. The pure integrator in the disturbance loop is kept to track DC-type or very low-frequency disturbances, owing to the infinite gain of the pure integrator at zero-frequency [31]. Moreover, the GIs of selective resonant frequencies are inserted in parallel in order to observe the FVSD of different frequencies.

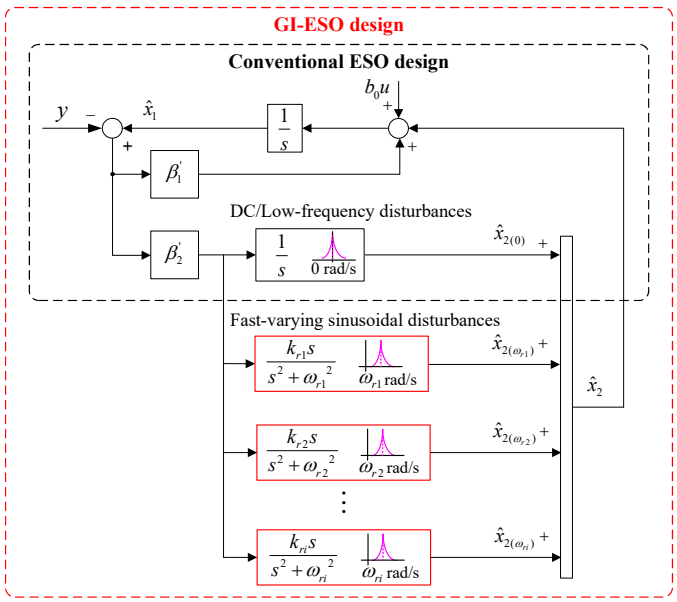

Fig. 7: Proposed GI-ESO design diagram

The inserted GI can be generally expressed by (14), wherein the infinite gain of the integrator is shifted to ω_{ri} [31].

$$R_i(s) = \frac{k_{ri}s}{s^2+\omega_{ri}^2},\ i = 1, 2, \dots \tag{14}$$

where k_{ri} is the proportional gain, and ω_{ri} is the selective resonant frequency of each GI.

A GI-ESO is extended from a conventional ESO (8) by

$$\begin{bmatrix}\dot{\hat{x}}_1\\ \dot{\hat{x}}_2\end{bmatrix} = \begin{bmatrix}0 & 1\\ 0 & 0\end{bmatrix}\begin{bmatrix}\hat{x}_1\\ \hat{x}_2\end{bmatrix} + \begin{bmatrix}b_0\\ 0\end{bmatrix}u + \begin{bmatrix}\beta_1^{'}\\ \beta_2^{'}(1+R(s)s)\end{bmatrix}[x_1 - \hat{x}_1] \tag{15}$$

where $\hat{x}_2 = \hat{x}_{2(0)} + \hat{x}_{2(\omega_{r1})} + \hat{x}_{2(\omega_{r2})} + \cdots + \hat{x}_{2(\omega_{ri})}$ is the total estimated disturbances, $R(s)$ is a general expression that is $R(s) = 0$ for ESO; $R(s) = R_1(s) + R_2(s) + \cdots + R_i(s)$ for GI-ESO. The observer gains are expressed by $\beta_1^{'} = \xi\omega_0$, $\beta_2^{'} = \omega_0^2$, and ξ is the tuning coefficient. Detailed theoretical analysis and selection guidelines are provided later in the sequel.

2) Estimation error assessment

Similarly, by subtracting (15) from (7), the estimation errors can be expressed by

$$\begin{bmatrix}\dot{e}_1\\ \dot{e}_2\end{bmatrix} = \begin{bmatrix}-\beta_1^{'} & 1\\ -\beta_2^{'}(1+R(s)s) & 0\end{bmatrix}\begin{bmatrix}e_1\\ e_2\end{bmatrix} + \begin{bmatrix}0\\ 1\end{bmatrix}h \tag{16}$$

By replacing h with $\dot{f}(s)$, the transfer function between $e_2(s)$ and $f(s)$ becomes:

$$F_{e_2}(s) = \frac{s(s+\xi\omega_o)}{s^2 + \xi\omega_o s + \omega_o^2(1+R(s)s)} \tag{17}$$

The bode plots of $F_{e_2}(s)$ are shown in Fig. 8, in which the disturbance estimation errors of ESO and GI-ESO are comparatively presented. For these two observers, the bandwidth is set to $\omega_o \in \{300, 400, 500\}$ (rad/s), and $\xi = 5$. The inserted GIs are respectively set to $k_{r1}, = \pi, \omega_{r1} = \omega_g$ for voltage offset, $k_{r2} = 5\pi, \omega_{r2} = 2\omega_g$ for unbalanced grids, $k_{r3} = 10\pi, \omega_{r3} = 6\omega_g$ for 5th-order and 7th-order harmonics (proven in Appendix A), and $\omega_g = 100\pi$ rad/s. The bode plots indicate that GI-ESO and ESO performs closely at either the very low-frequency or the high-frequency range. Moreover, being different from ESO, the proposed GI-ESO can also correctly track very FVSD. The reason is that the inserted GIs enable rather high gains at specific resonant frequencies.

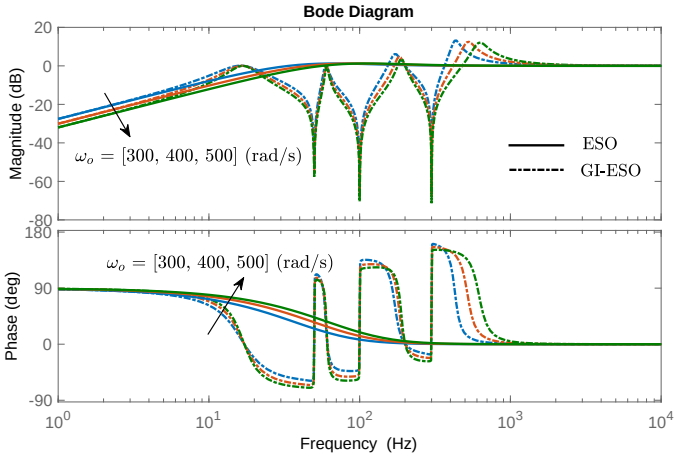

Fig. 8: Bode diagram of the transfer function $F_{e_2}(s)$

B. GI-ESO-based SRF-PLL design

The primary principles described in Section II-B are followed here, moreover, several particular points are highlighted.

1) Disturbances compensation

It has been proven in Section III-A that the proposed GI-ESO is capable of estimating very FVSDs. But another key question is how to correctly compensate the estimated disturbances. The GI-ESO-based SRF-PLL control diagram is shown in Fig. 9. The phase angle is indirectly estimated by controlling the q-axis voltage. If the total disturbances were compensated by the control signal $\Delta\omega$, the second-order frequency components would remain in the estimated frequency $\hat{\omega}$ and the output phase $\hat{\theta}$. Since the information of phase and frequency are more important in a PLL system. We can force the harmonics components to stay in the q-axis voltage (see Fig. 9). It comes from (3) that, the integration of $\hat{x}_{2(2\omega)}$ actually represents the v_{qe} fluctuations caused by unbalanced voltages. Finally, the sinusoidal errors can be actively removed from the output estimated phase.

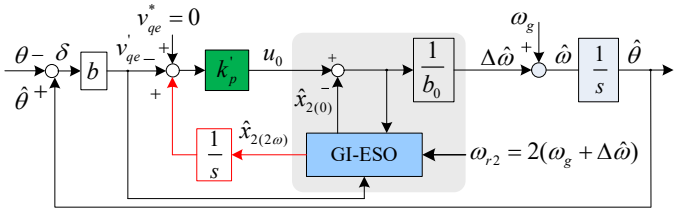

Fig. 9: GI-ESO-based SRF-PLL under voltage unbalances

2) Frequency-adaptive mechanism

Note that the actual grid frequency possibly derives from its nominal value ω_g [25]. If the resonant frequency of GI is set to be constant, then the performances of GI-ESO when used in GcCs can be deteriorated. A frequency-adaptive mechanism is hence considered in this design (see Fig. 9). For example, under voltage unbalances, the value of the resonant frequency of GI is adaptively adjusted by considering the estimated frequency deviation with $\omega_{r2} = 2(\omega_g + \Delta\hat{\omega})$. As the applied resonant frequencies of GIs are corrected in real-time, the negative effects induced by frequency deviations can be significantly mitigated.

3) Control law formulation

The DC-type or low-frequency disturbances $\hat{x}_{2(0)}$ are directly compensated in the signal u_0. The integration of $\hat{x}_{2(2\omega)}$ is added to the q-axis voltage reference. Finally, the modified control law is expressed by

$$\Delta\hat{\omega} = \frac{k_p^{'}(v_{qe}^{*} + \int \hat{x}_{2(2\omega)}dt - v_{qe}^{'}) - \hat{x}_{2(0)}}{b_0} \tag{18}$$

The GI-ESO handles all sinusoidal components that are present in the SRF-PLL as generalized disturbances. The structure of GI-ESO can be flexibly adapted to different disturbed regimes by adjusting the selective frequencies.

4) Stability analysis

The stability index is a crucial factor for evaluating the quality of a controller. Stabilities analysis methods of ESO can be referred for that of GI-ESO [35]–[37]. The frequency domain properties are therefore quantitatively analyzed in this section. This is done under the following assumptions:

- A mismatch between b and b_0 is assumed, the control gain is set to be $b = 1.2$, and $b_0 = 1$.
- The parameters k_{r1} and ω_{r1} are defined as the proportional gain and the resonant frequency for the GI dealing with voltage offsets, similarly, ω_{r2} and k_{r2} for voltage unbalances, ω_{r3} and k_{r3} for harmonics.
- Phase margins around 45° are supposed to be acceptable.

From expressions (15) and (18), the transfer function can be obtained:

$$\frac{u(s)}{y(s)} = -\frac{1}{b_0}\frac{\omega_c s^2 + {\omega_o}^2 s + \xi\omega_o\omega_c s + {\omega_o}^2\omega_c}{s(s+\xi\omega_o) + {\omega_o}^2(s+\omega_c)R(s)} \tag{19}$$

$$\frac{u(s)}{r(s)} = \frac{1}{b_0}\frac{\omega_c s^2 + {\omega_o}^2\omega_c R(s)s + \xi\omega_o\omega_c s + {\omega_o}^2\omega_c}{s(s+\xi\omega_o) + {\omega_o}^2(s+\omega_c)R(s)} \tag{20}$$

where $r(s)$, $u(s)$, and $y(s)$ are the Laplace transforms of $r = v_{qe}^{*}$, $u = \Delta\hat{\omega}$, and $y = v_{qe}^{'}$, respectively.

By introducing the following notations:

$$C(s) = \frac{1}{b_0}\frac{\omega_c s^2 + {\omega_o}^2 s + \xi\omega_o\omega_c s + {\omega_o}^2\omega_c}{s(s+\xi\omega_o) + {\omega_o}^2(s+\omega_c)R(s)} \tag{21}$$

$$H(s) = \frac{\omega_c s^2 + {\omega_o}^2\omega_c R(s)s + \xi\omega_o\omega_c s + {\omega_o}^2\omega_c}{\omega_c s^2 + {\omega_o}^2 s + \xi\omega_o\omega_c s + {\omega_o}^2\omega_c} \tag{22}$$

the ESO-based controller can be formulated to a two-degree-of-freedom (2dof) closed-loop system as shown in Fig. 10. Now, the feedback control loop has a standard structure of the feedback and the controlled plant [37].

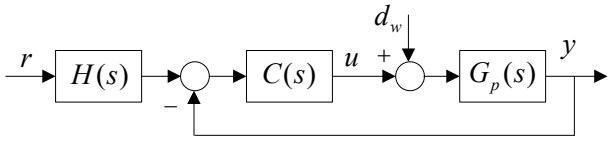

Fig. 10: 2dof closed-loop diagram of GI-ESO-based SRF-PLL control system, d_w represents external disturbances

Firstly, the phase margins of the loop transfer function of the controlled system are discussed. The loop transfer function is given by:

$$\begin{aligned} L(s) &= C(s)G_p(s) \\ &= \frac{1}{b_0}\frac{\omega_c s^2 + {\omega_o}^2 s + \xi\omega_o\omega_c s + {\omega_o}^2\omega_c}{s(s+\xi\omega_o) + {\omega_o}^2(s+\omega_c)R(s)}\frac{b}{s} \end{aligned} \tag{23}$$

where the plant model is $G_p(s) = b/s$, and $b = V_m/v_{de}$.

The unbalanced voltage case is exclusively studied in order to analyze the effects on stability with respect to each parameter $(\xi, \omega_o, \omega_c, k_r)$. The bode plots of $L(s)$ for different coefficients $\xi \in \{2, 3, 4\}$ are shown in Fig. 11. The remaining parameters are set to $\omega_o = 400$ rad/s, $\omega_c = 100$ rad/s, $k_{r2} = 5\pi$, $\omega_{r2} = 2\omega_g$. It can be observed that the gain margin is negative infinitive, however, the phase margin cannot sufficiently meet stabilities requirements for $\xi = 2$ or $\xi = 3$. While too large ξ enables slow dynamics response [4]. Therefore, $\beta_1^{'} = 4\omega_0$ and $\beta_2^{'} = \omega_0^2$ are chosen in this work as well as in the forthcoming analysis.

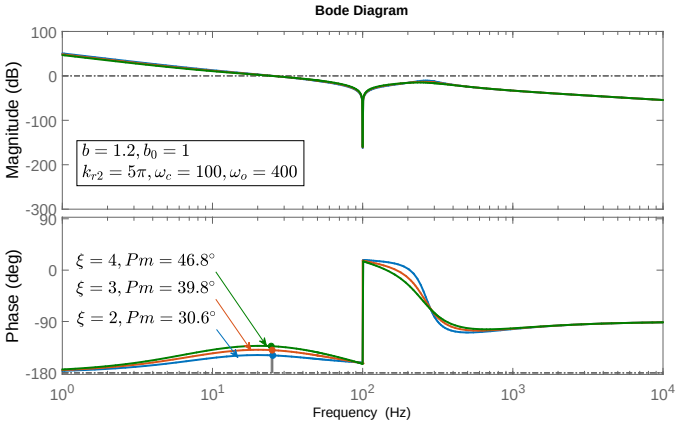

Fig. 11: Bode plots of $L(s)$ for coefficient $\xi \in \{2, 3, 4\}$

The bode plots of $L(s)$ for different ω_o and ω_c are shown in Figs. 12 and 13, respectively. The GI is applied with $k_{r2} = 5\pi$, and $\omega_{r2} = 2\omega_g$. The ESO's tuning rule can be referred, that is commonly configured by $\omega_o = 3 \sim 5\omega_c$ [4]. Then, we make the following settings: $\omega_o \in \{300, 400, 500\}$ (rad/s), $\omega_c = 100$ rad/s for Fig. 12; $\omega_o = 400$ (rad/s), $\omega_c \in \{80, 100, 120\}$ (rad/s) for Fig. 13. It can be seen that the phase margin will decrease with larger observer bandwidth ω_o, which can deteriorate stabilities of the closed-loop control system. However, the phase margins are insensitive to the changes of ω_c.

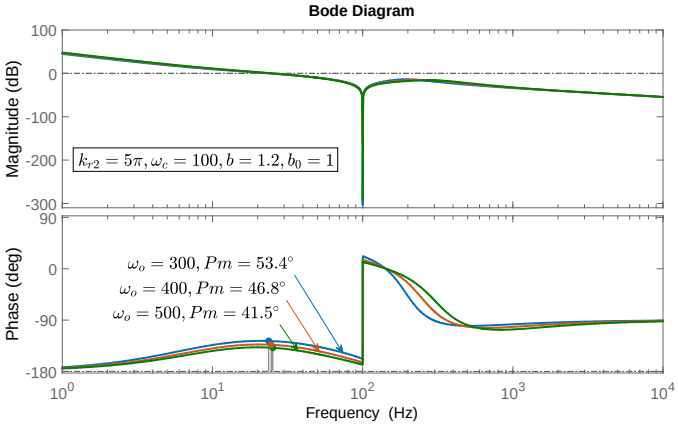

Fig. 12: Bode plots of $L(s)$ for $\omega_o \in \{300, 400, 500\}$ (rad/s)

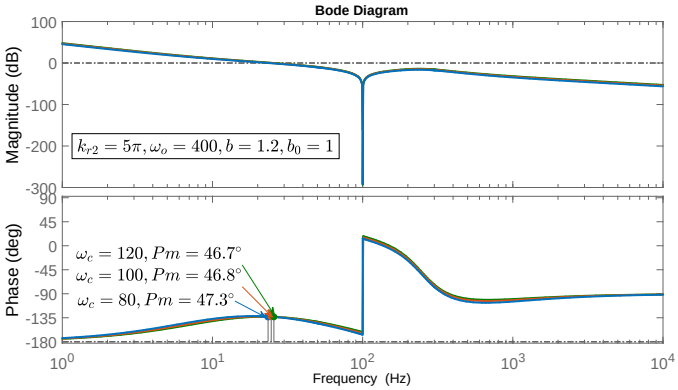

Fig. 13: Bode plots of $L(s)$ for $\omega_c \in \{80, 100, 120\}$ (rad/s)

The bode plots of $L(s)$ of different k_{r2} are shown in Fig. 14. The GIs are set to $k_{r2} \in \{\pi, 5\pi, 10\pi\}$, and $\omega_{r2} = 2\omega_g$. Larger k_{r2} enables higher gains of GI at the selective frequencies which helps improving the estimation accuracy of GI-ESO. However, the phase margins are sensitive to the changes of k_{r2} as shown in Fig. 14. The high gains tend to bring destabilizing effects on the resulting closed-loop system. Too large gains would be risky in respect to stability issues. Consequently, the gains of inserted GI are limited accordingly.

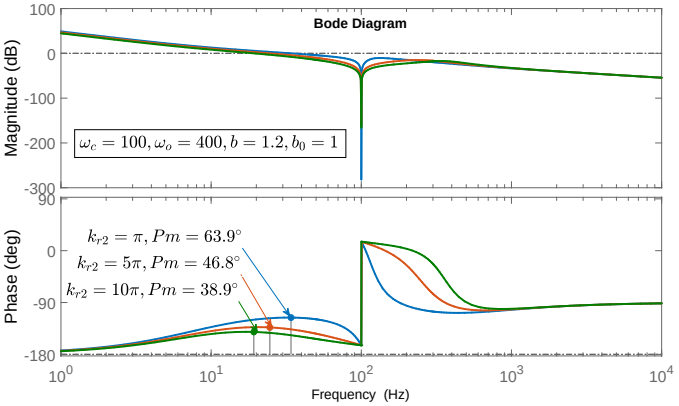

Fig. 14: Bode plots of $L(s)$ for $k_{r2} \in \{\pi, 5\pi, 10\pi\}$

Now, the stabilities of GI-ESOs with different selective frequencies are analyzed. The resonant frequencies of applied GIs are respectively configured with $\omega_{r1} = \omega_g$ for voltage offset, $\omega_{r2} = 2\omega_g$ for grid unbalance, and $\omega_{r3} = 6\omega_g$ for 5th-order and 7th-order harmonics (see Appendix A).

The bode plots of $L(s)$ for different selective frequencies are provided in Fig. 15. The same gains of GIs with $k_{r1} = k_{r2} = k_{r3} = 5\pi$ are used. It can be seen that the phase margin decreases critically for system that applies a GI with lower resonant frequency. Therefore, the gains of GIs must be selected by taking into account its applied resonant frequency.

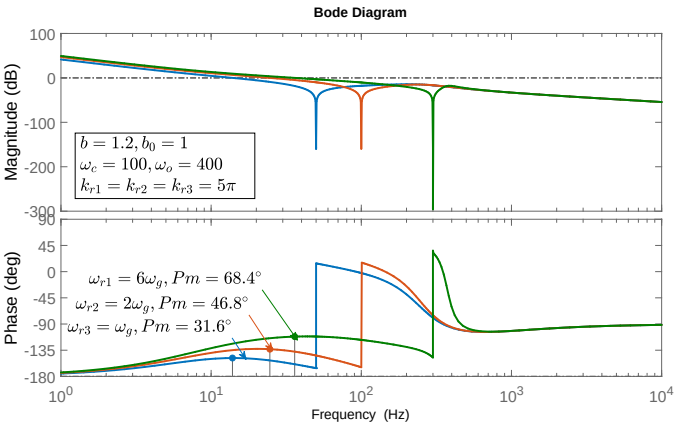

Fig. 15: Bode plots of $L(s)$ for various selective frequencies

Fig. 16 shows the bode plots of $L(s)$ that apply different gains k_{ri}, the remaining parameters keep the same configurations. Compared to the ESO, although the stability margins decrease due to the high gains of GIs, the stability condition can be ensured by properly adjusting k_{ri}.

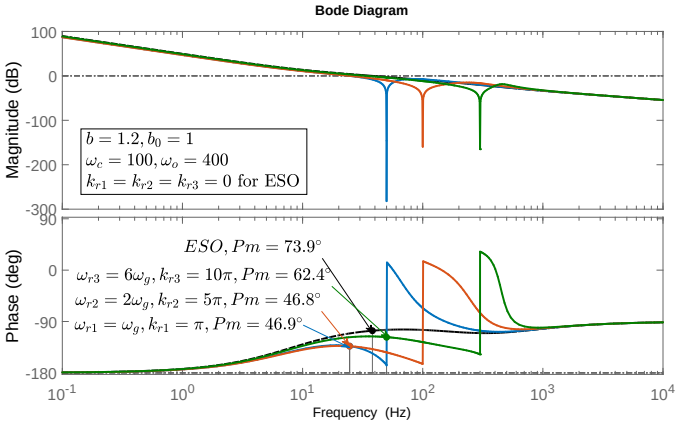

Fig. 16: Bode plots of $L(s)$ for different k_{ri}

The bode plots of $L(s)$ for multi-GIs in parallel are provided in Fig. 17, with the same parameters settings as that applied in Fig. 16. It can be observed that multi-GIs cause a further decrease of phase margin ($\xi = 4, P_m = 38.3°$). The coefficient ξ is thus adjusted by using $\xi = 5$ for multi-GIs to ensure that the stability margin is sufficient.

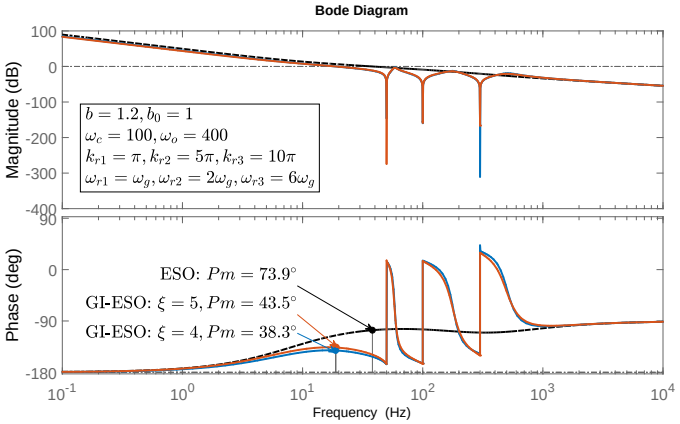

Fig. 17: Bode plots of $L(s)$ for multiple selective frequencies

The control system performances and stability can be affected by model uncertainties. The main uncertain parameter is the control gain b. The estimation of b is set to $b_0 = 1$, the control robustness with a group of values $b \in \{0.5, 1, 1.5\}$ are successively tested. The Bode plots of the loop transfer function $L(s)$ for different b are provided in Fig. 18. The phase margin decreases when b_0 is far from the real value of b. However, the phase margin are insensitive to variations of b and remains always practically accepted ($P_m > 40°$).

The stability of the pre-filter $H(s)$ (22) is guaranteed, as all coefficients in its denominator are positive [35]. Therefore, the closed-loop stability of the loop that linked the synthesized reference signal $r^* = \int \hat{x}_{2(2\omega)} dt + v_{qe}^*$ to the output can be determined by

$$G_{cl}(s) = \frac{C(s)G_p(s)}{1 + C(s)G_p(s)} \tag{24}$$

The bode plots of $G_{cl}(s)$ are shown in Fig. 19, the same parameters are configured as that of Fig. 17. The bode plots

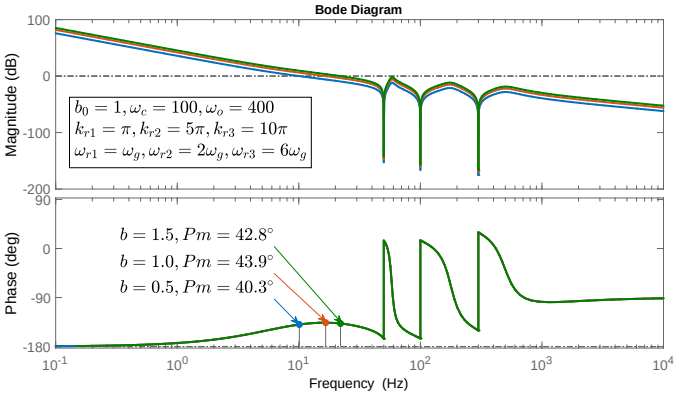

Fig. 18: Bode plots of $L(s)$ for $b \in \{0.5, 1, 1.5\}$

show that GI-ESO inherits the ESO's original properties. The closed-loop performances of ESO- and GI-ESO- based control system behave closely at either very low-frequency or high-frequency range. Moreover, by using a GI-ESO, the selective sinusoidal disturbances are effectively removed from the control signal as well as the output estimated phase.

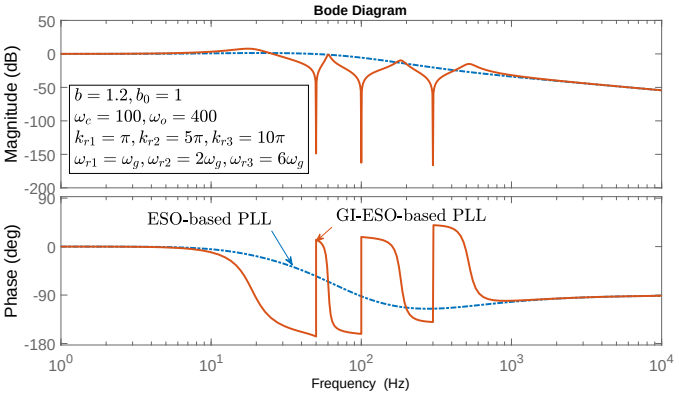

Fig. 19: Bode bolts of closed-loop transfer function $G_{cl}(s)$

This part provides a general stability analysis methodology, which can be adapted to future implementations of GI-ESOs.

6) Parameter selection guidelines

Firstly, the structure and the selective frequencies of GI-ESOs need to be adapted to the sinusoidal disturbances present in a real applications. Then, proper parameters have to be selected by taking into account several factors: system stability, estimation's precision and response dynamics. The parameter tuning guidelines are summarized as follow:

- Firstly, regarding parameters ω_c and ω_0, similar tuning rules discussed in [4], [7] can be followed.
- Then, ω_{ri} is chosen by adapting to frequencies of the present sinusoidal disturbances, and k_{ri} is tuned to ensure both the estimation precision and the stability.
- Moreover, the coefficient ξ have to be corrected for GI-ESO to ensure the stability condition.
- Finally, the applied control parameters must be retuned and validated in the experimental tests.

Finally, the control parameters are configured as given in Table I, which will be validated in the forthcoming tests.

TABLE I: Configurations of control parameters

Common parameters	$\omega_c = 100$ rad/s, $\omega_o = 400$ rad/s, $b_0 = 1$
Coefficient ξ	$\xi = 4$ for single GI, $\xi = 5$ for multi-GIs
Offsets	$k_{r1} = \pi$, $\omega_{r1} = (\omega_g + \Delta\hat{\omega})$
Unbalances	$k_{r2} = 5\pi$, $\omega_{r2} = 2(\omega_g + \Delta\hat{\omega})$
Harmonics	$k_{r3} = 10\pi$, $\omega_{r3} = 6(\omega_g + \Delta\hat{\omega})$

IV. Experimental Results and Analysis

The GI-ESO-based SRF-PLL is tested in order to check the effectiveness of the proposed GI-ESO in dealing with FVSD. Various disturbed schemes (unbalances, harmonics, and voltage offset) have been considered. Experimental results are obtained by using the dSPACE controller (DS2005).

First of all, the grid unbalances are set to be the same as the settings in Fig. 5. The performances of GI-ESO-based PLL are shown in Fig. 20. By introducing the GI, the second-order grid frequency disturbance is approximately estimated by the GI-ESO, namely $\hat{x}_{2(2\omega)} \approx d_{(2\omega)}$. Then, the fluctuations are actively transmitted to the q-axis voltage. Fig. 21 shows that the integration of $\hat{x}_{2(2\omega)}$ enables a tight tracking of the desired theoretical value $\Delta v_{qe(2\omega)}$. The sinusoidal components are forced to remain in the q-axis voltage. Finally, the errors are removed from the estimating phase angle. The performances are significantly improved compared with the ESO-based PLL (see Fig. 6 for comparison).

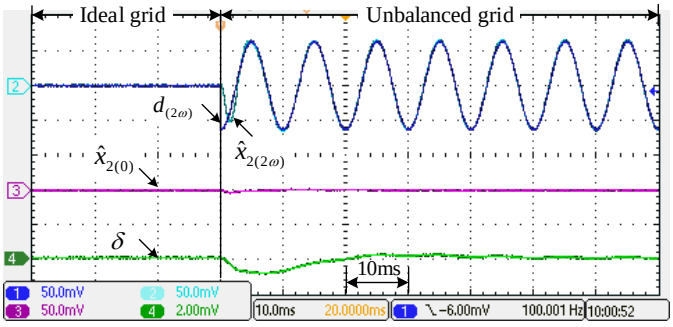

Fig. 20: Performance of GI-ESO-based PLL, $d_{(2\omega)}$ the sinusoidal disturbances (50/div), $\hat{x}_{2(2\omega)}$ the estimated sinusoidal disturbances (50/div), $\hat{x}_{2(0)}$ the estimated DC-type or low-frequency disturbances (50/div), δ the phase error (2°/div)

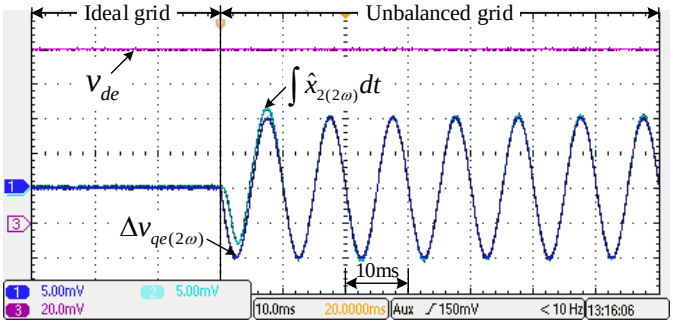

Fig. 21: Voltage components in the dq frame, $\Delta v_{qe}(2\omega)$ the fluctuations of q-axis voltage ($5V$/div), $\int \hat{x}_{2(2\omega)} dt$ the integration of $\hat{x}_{2(2\omega)}$ ($5V$/div), v_{de} the d-axis voltage ($20V$/div)

Fig. 22 provides the robustness test results of GI-ESO-based PLL for two cases: the three-phase voltages undergo a phase jump ($+10°$) as shown in Fig. 22 (a); a grid frequency step ($+3Hz$) occurs to the grid voltages as shown in Fig. 22 (b). The GI-ESO can quickly track the sinusoidal disturbances when the external disturbances present to the grid voltage for both occasions. Moreover, the GI-ESO have a fast enough tracking performance to ensure that the control of GI-ESO-based PLL can achieve a rapid dynamic response.

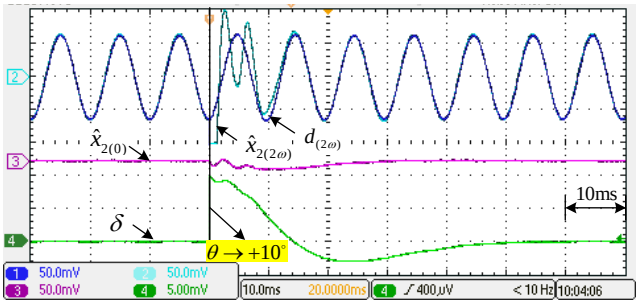

(a) Phase jump $+10°$

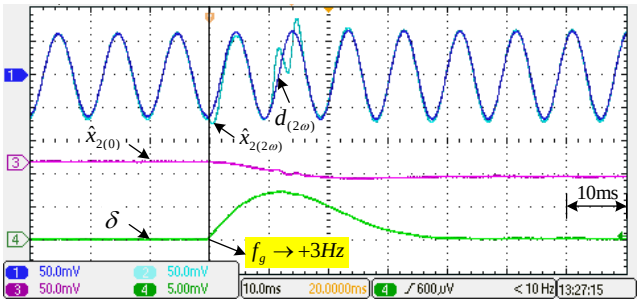

(b) Frequency step $+3Hz$

Fig. 22: Robustness test of a GI-ESO-based PLL, $d_{(2\omega)}$ the sinusoidal disturbances (50/div), $\hat{x}_{2(2\omega)}$ the estimated sinusoidal disturbance (50/div), $\hat{x}_{2(0)}$ the estimated low-frequency disturbance (50/div), δ the phase error (5°/div)

The voltage offset is set to $V_{ao} = 0V$, $V_{bo} = V_{bo} = 10V$ (parameters are defined in Appendix A), the control parameters are given in Table I. The performance of GI-ESO and the resulting PLL under voltage offset are shown in Fig. 23.

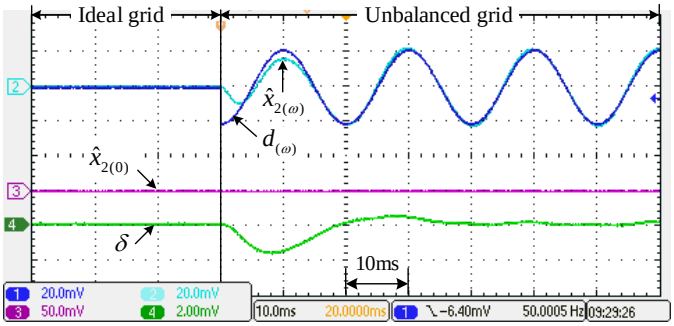

Fig. 23: Performance of GI-ESO-based PLL in presence of voltage offset, $d_{(\omega)}$ the sinusoidal disturbances (50/div), $\hat{x}_{2(\omega)}$ the estimated sinusoidal disturbances (50/div), $\hat{x}_{2(0)}$ the estimated DC or low-frequency disturbances (50/div), δ the phase error (2°/div)

The sinusoidal disturbances induced by voltage offset have the same frequency component as that of grid voltage [24]. As shown in Fig. 23, the results indicate that the sinusoidal disturbances are tightly tracked by GI-ESO. The PLL enables the performance precision regarding voltage offsets.

Regarding harmonics regime, the 5th-order harmonic of magnitude $10V$ and the 7th-order harmonic of magnitude $5V$ are injected simultaneously into three-phase voltages. The 6th-order harmonic disturbances appear in the SRF-PLL control system (proven in Appendix A). The control parameters are given in Table I. Fig. 24 shows that the harmonic disturbances are approximately estimated by GI-ESO. The high-order harmonic errors in the estimated phase become negligible.

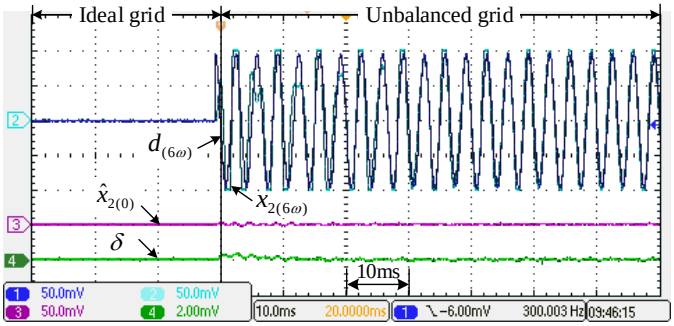

Fig. 24: Performance of GI-ESO-based PLL in presence of harmonics disturbances, $d_{(6\omega)}$ the 6th-order harmonic disturbances (50/div), $\hat{x}_{2(6\omega)}$ the estimated 6th-order harmonic disturbances (50/div), $\hat{x}_{2(0)}$ the estimated DC or low-frequency disturbances (50/div), δ the phase error (2°/div)

For a real application, the PLLs are expected to be robust against unbalances, offsets, and harmonics. Fig. 25 provides the results of GI-ESO-based PLL that deal with various disturbances simultaneously. Multi-GIs of different resonant frequencies are incorporated in parallel, being configured in Table I. The total multi-disturbances can be identified by the GI-ESO. The overshoot of estimated phase angle is less than 1.1%, and the estimated phase quickly follow the phase of grid voltage. The proposed GI-ESO-based PLL achieves practically satisfied performances in presence of various disturbances.

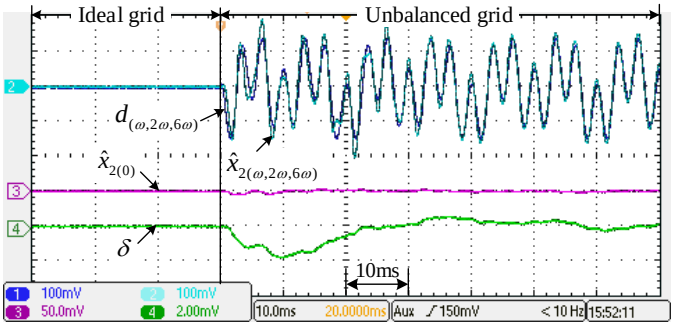

Fig. 25: Performance of GI-ESO-based PLL in presence of multi-harmonic disturbances, $d_{2(\omega,2\omega,6\omega)}$ the multi-harmonic disturbances (100/div), $\hat{x}_{2(\omega,2\omega,6\omega)}$ the estimated disturbances (100/div), $\hat{x}_{2(0)}$ the estimated DC or low-frequency disturbances (50/div), δ the phase error (2°/div)

Fig. 26 shows the results of GI-ESO-based PLL in presence of grid frequency deviation ($+3Hz$). The comparative results indicate that the magnitude of estimated phase errors decrease by introducing the frequency-adaptive mechanism.

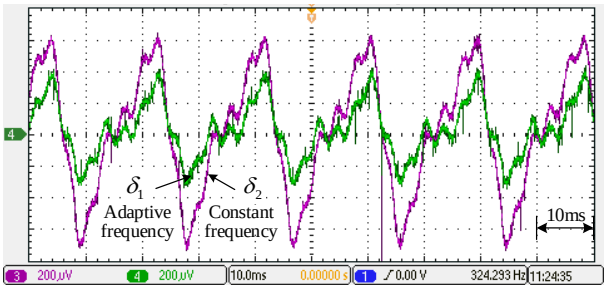

Fig. 26: Phase estimation errors in presence of grid frequency deviation, δ_1 the phase error with adaptive frequency (0.02°/div), δ_2 the phase error with fixed frequency (0.02°/div)

In this paper, the presented results are focused on PLL issues. However, the proposed GI-ESO can be used in other applications that might be encountered in GcCs like the DC-link control or the grid current control contexts. These are topics of undergoing works.

V. Conclusions

This work is a development/extension of a previously proposed work on linear ESO, therefore, it inherits the ESO's original advantages. Moreover, GIs of different resonant frequencies are applied into the disturbance estimation loop, which enables FVSD to be observed with a relatively low bandwidth. Besides, a frequency-adaptive mechanism is introduced in order to mitigate the effects of frequency deviations. Furthermore, the structure of GI-ESO can be flexibly adjusted regarding different disturbed regimes present on the field.

A case of three-phase SRF-PLL control system is chosen as an example to assess GI-ESO's performance and the stability of its resulting control system. Firstly, the frequency domain properties, particularly the phase margins are quantitatively analyzed with respect to different control parameters. The parameters tuning guidelines are highlighted as well. Moreover, the experimental results indicate that various FVSD can be efficiently observed by introducing GI-ESOs. The sinusoidal components are removed from the estimated phase angle by compensating correctly the estimated disturbances. Besides, in the case of frequency deviations, the frequency-adaptive mechanism mitigates the phase estimation errors. The GI-ESO also achieves high robustness under various internal or external disturbances. Both theoretical analysis and experimental results have proven the effectiveness of the proposed solution when used in GcCs in presence of various disturbances.

The proposed GI-ESO solution breaks the limits of ESO-based controllers or ADRC for their applications in various disturbed control schemes of GcCs (grid synchronization, current control, and DC-link voltage control). Moreover, it has a wide applications scope for many systems are impacted by the presence of very FVSD. If the frequencies of sinusoidal disturbances are not known, a simple PLL can be incorporated to obtain the frequency information.

APPENDIX A
ERROR ANALYSIS AND DISTURBANCES DEFINITION

The error analysis of voltage harmonics and offset are recalled in order to define the disturbances present in the control system of GI-ESO-based SRF-PLL.

A.1. *Voltage harmonics*

The grid voltages with harmonics can be represented by:

$$\begin{aligned} v_a =& V_1\cos\theta + V_5\cos 5\theta + V_7\cos 7\theta + \dots \\ v_b =& V_1\cos(\theta-\frac{2\pi}{3}) + V_5\cos 5(\theta-\frac{2\pi}{3}) \\ &+ V_7\cos 7(\theta-\frac{2\pi}{3}) + \dots \\ v_c =& V_1\cos(\theta+\frac{2\pi}{3}) + V_5\cos 5(\theta+\frac{2\pi}{3}) \\ &+ V_7\cos 7(\theta+\frac{2\pi}{3}) + \dots \end{aligned} \tag{25}$$

where V_1, V_5, V_7, ... represent the harmonics magnitudes.

The q-axis voltage can be derived and linearised by:

$$\begin{aligned} v_{qe} &= V_1\sin\delta + V_5\sin(\hat{\theta}+5\theta) + V_7\sin 7(\hat{\theta}-7\theta) + \dots \\ &\approx V_1\delta + (V_5-V_7)\sin 6\theta + (V_{11}-V_{13})\sin 12\theta + \dots \end{aligned} \tag{26}$$

The phase error caused by voltage harmonics is given by

$$\delta = E_{6\omega}\sin 6\theta + E_{12\omega}\sin 12\theta + \dots \tag{27}$$

where

$$E_{6\omega} = \frac{V_5-V_7}{V_1}, \quad E_{12\omega} = \frac{V_{11}-V_{13}}{V_1}, \dots .$$

The voltage harmonics enables the phase errors with the frequency components of 6ω, 12ω, ..., . The total disturbance of ESO-based PLL control system can be represented by:

$$\begin{aligned} f =& [(b-b_0)\Delta\hat{\omega} + (\omega_g-\omega) + d_x] + \\ & 6\omega E_{6\omega}\cos 6\theta + 12\omega E_{12\omega}\cos 12\theta + \dots \end{aligned} \tag{28}$$

A.2. *Voltage offset*

The measurement offset or the signal conversion circuits can sometimes cause voltage offset [24]. The unbalanced grid voltages can be represented by:

$$\begin{aligned} v_a &= V_m\cos\theta + V_{ao} \\ v_b &= V_m\cos(\theta-\frac{2\pi}{3}) + V_{bo} \\ v_c &= V_m\cos(\theta+\frac{2\pi}{3}) + V_{co} \end{aligned} \tag{29}$$

where V_{ao}, V_{bo}, and V_{co} represent the offset voltage levels.

The voltages in the $\alpha\beta$ frame are as follows:

$$\begin{aligned} v_\alpha &= V_m\cos\theta + V_{\alpha o} \\ v_\beta &= V_m\cos\theta + V_{\beta o} \end{aligned} \tag{30}$$

where $V_{\alpha o} = \frac{2}{3}(V_{ao}+V_{bo}+V_{co})$, $V_{\beta o} = \frac{1}{\sqrt{3}}(V_{co}-V_{bo})$.

The q-axis voltage can be derived and linearised by:

$$\begin{aligned} v_{qe} &= V_m\sin\delta + V_{\alpha 0}\sin\hat{\theta} + V_{\beta 0}\cos\hat{\theta} \\ &\approx V_m\delta + E_\omega\cos(\theta+\phi_0) \end{aligned} \tag{31}$$

where

$$E_\omega = \sqrt{V_{\alpha 0}^2 + V_{\beta 0}^2}, \quad \phi_0 = -\tan^{-1}\left(\frac{V_{\alpha 0}}{V_{\beta 0}}\right).$$

The phase error caused by the offset has the same frequency component as that of the grid voltage [24]. The phase error caused by the voltage offset is given by:

$$\delta = \frac{E_\omega}{V_m}\cos(\theta+\phi_0) \tag{32}$$

The total disturbances present in ESO-based PLL control system can be expressed by:

$$f = [(b-b_0)\Delta\hat{\omega} + (\omega_g-\omega) + d_x] + \omega\frac{E_\omega}{V_m}\sin(\theta+\phi_0) \tag{33}$$

REFERENCES

[1] J. Chen, R. J. Patton, and H. Zhang, "Design of unknown input observers and robust fault detection filters," *International Journal of Control*, vol. 63, no. 1, pp. 85–105, 1996.

[2] W. Chen, J. Yang, L. Guo, and S. Li, "Disturbance-Observer-Based Control and Related Methods - An Overview," *IEEE Transactions on Industrial Electronics*, vol. 63, no. 2, pp. 1083–1095, Feb 2016.

[3] J. Han, "From PID to active disturbance rejection control," *IEEE transactions on Industrial Electronics*, vol. 56, no. 3, pp. 900–906, 2009.

[4] Z. Gao, "Scaling and bandwidth-parameterization based controller tuning," in *Proceedings of the American control conference*, vol. 6, 2006, pp. 4989–4996.

[5] R. Madoński and P. Herman, "Survey on methods of increasing the efficiency of extended state disturbance observers," *ISA Transactions*, vol. 56, pp. 18 – 27, 2015.

[6] Y. Huang and W. Xue, "Active disturbance rejection control: Methodology and theoretical analysis," *ISA Transactions*, vol. 53, no. 4, pp. 963 – 976, 2014, disturbance Estimation and Mitigation.

[7] B. Guo, S. Bacha, M. Alamir, A. Mohamed, and C. Boudinet, "LADRC applied to variable speed micro-hydro plants: Experimental validation," *Control Engineering Practice*, vol. 85, pp. 290 – 298, 2019.

[8] B. Guo, S. Bacha, and M. Alamir, "A review on ADRC based PMSM control designs," in *IECON 2017 - 43rd Annual Conference of the IEEE Industrial Electronics Society*, Oct 2017, pp. 1747–1753.

[9] B. Guo and Z. Zhao, "On the convergence of an extended state observer for nonlinear systems with uncertainty," *Systems Control Letters*, vol. 60, no. 6, pp. 420 – 430, 2011.

[10] D. Yoo, S. S. . Yau, and Z. Gao, "On convergence of the linear extended state observer," in *2006 IEEE International Conference on Control Applications*, Oct 2006, pp. 1645–1650.

[11] Q. Zheng, L. Q. Gao, and Z. Gao, "On stability analysis of active disturbance rejection control for nonlinear time-varying plants with unknown dynamics," in *2007 46th IEEE Conference on Decision and Control*, Dec 2007, pp. 3501–3506.

[12] A. A. Godbole, J. P. Kolhe, and S. E. Talole, "Performance Analysis of Generalized Extended State Observer in Tackling Sinusoidal Disturbances," *IEEE Transactions on Control Systems Technology*, vol. 21, no. 6, pp. 2212–2223, Nov 2013.

[13] B. Sun and Z. Gao, "A DSP-based active disturbance rejection control design for a 1-kW H-bridge DC-DC power converter," *IEEE Transactions on Industrial Electronics*, vol. 52, no. 5, pp. 1271–1277, 2005.

[14] R. Miklosovic, A. Radke, and Z. Gao, "Discrete implementation and generalization of the extended state observer," in *2006 American Control Conference*, June 2006, pp. 6 pp.–.

[15] J. Cortés-Romero, A. Luviano-Juarez, and H. Sira-Ramirez, "Robust GPI controller for trajectory tracking for induction motors," in *2009 IEEE International Conference on Mechatronics*, April 2009, pp. 1–6.

[16] J. Cortés-Romero, G. A. Ramos, and H. Coral-Enriquez, "Generalized proportional integral control for periodic signals under active disturbance rejection approach," *ISA Transactions*, vol. 53, no. 6, pp. 1901 – 1909, 2014.

[17] G. Ramos, J. Cortés-Romero, and H. Coral-Enriquez, "Spatial observer-based repetitive controller: An active disturbance rejection approach," *Control Engineering Practice*, vol. 42, pp. 1 – 11, 2015.

[18] K. K. Busawon and P. Kabore, "Disturbance attenuation using proportional integral observers," *International Journal of Control*, vol. 74, no. 6, pp. 618–627, 2001.

[19] M. Andreica, S. Bacha, D. Roye, I. Munteanu, A. I. Bratcu, and J. Guiraud, "Cross-flow water turbines control under grid disturbances," in *2009 IEEE Bucharest PowerTech*, June 2009, pp. 1–6.
[20] G. Wu, L. Sun, and K. Y. Lee, "Disturbance rejection control of a fuel cell power plant in a grid-connected system," *Control Engineering Practice*, vol. 60, pp. 183 – 192, 2017.
[21] R. M. Santos Filho, P. F. Seixas, P. C. Cortizo, L. A. B. Torres, and A. F. Souza, "Comparison of Three Single-Phase PLL Algorithms for UPS Applications," *IEEE Transactions on Industrial Electronics*, vol. 55, no. 8, pp. 2923–2932, Aug 2008.
[22] M. H. J. Bollen, "Voltage Recovery after Unbalanced and Balanced Voltage Dip in Three-Phase Systems," *IEEE Power Engineering Review*, vol. 22, no. 10, pp. 63–64, Oct 2002.
[23] I. Etxeberria-Otadui, A. L. D. Heredia, H. Gaztanaga, S. Bacha, and M. R. Reyero, "A Single Synchronous Frame Hybrid (SSFH) Multi-frequency Controller for Power Active Filters," *IEEE Transactions on Industrial Electronics*, vol. 53, no. 5, pp. 1640–1648, Oct 2006.
[24] S.-K. Chung, "A phase tracking system for three phase utility interface inverters," *IEEE Transactions on Power Electronics*, vol. 15, no. 3, pp. 431–438, May 2000.
[25] H. Bevrani, A. Ghosh, and G. Ledwich, "Renewable energy sources and frequency regulation: survey and new perspectives," *IET Renewable Power Generation*, vol. 4, no. 5, pp. 438–457, Sep. 2010.
[26] M. Tsili and S. Papathanassiou, "A review of grid code technical requirements for wind farms," *IET Renewable Power Generation*, vol. 3, no. 3, pp. 308–332, Sep. 2009.
[27] S. Golestan, J. M. Guerrero, and J. C. Vasquez, "Three-Phase PLLs: A Review of Recent Advances," *IEEE Transactions on Power Electronics*, vol. 32, no. 3, pp. 1894–1907, March 2017.
[28] B. Guo, S. Bacha, M. Alamir, C. Boudinet, and H. Mesnage, "An enhanced phase-locked loop with extended state observer," in *2019 20th International Symposium on Power Electronics (Ee)*, Oct 2019, pp. 1–6.
[29] P. Rodriguez, J. Pou, J. Bergas, J. I. Candela, R. P. Burgos, and D. Boroyevich, "Decoupled Double Synchronous Reference Frame PLL for Power Converters Control," *IEEE Transactions on Power Electronics*, vol. 22, no. 2, pp. 584–592, March 2007.
[30] S. Golestan, M. Ramezani, J. M. Guerrero, F. D. Freijedo, and M. Monfared, "Moving Average Filter Based Phase-Locked Loops: Performance Analysis and Design Guidelines," *IEEE Transactions on Power Electronics*, vol. 29, no. 6, pp. 2750–2763, June 2014.
[31] Z. Xin, R. Zhao, P. Mattavelli, P. C. Loh, and F. Blaabjerg, "Re-Investigation of Generalized Integrator Based Filters From a First-Order-System Perspective," *IEEE Access*, vol. 4, pp. 7131–7144, 2016.
[32] D. N. Zmood and D. G. Holmes, "Stationary frame current regulation of pwm inverters with zero steady state error," in *30th Annual IEEE Power Electronics Specialists Conference. Record. (Cat. No.99CH36321)*, vol. 2, July 1999, pp. 1185–1190 vol.2.
[33] B. Guo, S. Bacha, M. Alamir, and H. Boudinet, "A Robust LESO-based DC-Link Voltage Controller for Variable Speed Hydro-Electric Plants," in *2019 IEEE International Conference on Industrial Technology (ICIT)*, Feb 2019, pp. 361–366.
[34] J. Tatsumi and Z. Gao, "On the enhanced ADRC design with a low observer bandwidth," in *Proceedings of the 32nd Chinese Control Conference*, July 2013, pp. 297–302.
[35] G. Tian and Z. Gao, "Frequency response analysis of active disturbance rejection based control system," in *2007 IEEE International Conference on Control Applications*, Oct 2007, pp. 1595–1599.
[36] S. Zhong and Y. Huang, "Comparison of the Phase Margins of Different ADRC Designs," in *2019 Chinese Control Conference (CCC)*, July 2019, pp. 1280–1285.
[37] H. Jin, J. Song, S. Zeng, and W. Lan, "Linear active disturbance rejection control tuning approach guarantees stability margin," in *2018 15th International Conference on Control, Automation, Robotics and Vision (ICARCV)*, Nov 2018, pp. 1132–1136.

Baoling Guo received the B.S and M.S. degrees from the China University of Petroleum, Qingdao, China, in 2012 and 2014, respectively, and the M.S. degree from the Grenoble Institute of Technology (INPG), Grenoble, France, in 2015, and the Ph.D. degree from Grenoble Electrical Engineering Laboratory (G2Elab), University Grenoble Alpes, Grenoble, France, in 2019. Her main research interests include variable speed hydropower generation, power electronics system modelling and control, and renewable energy integration.

Seddik Bacha received the B.S. and M.S. degrees from the Ecole Nationale Polytechnique d'Alger, Algiers, Algeria, in 1982 and 1990, respectively, and the Ph.D. degree from the Grenoble Institute of Technology (INPG), Grenoble, France, in 1993. In 1990, he joined the Laboratoire d'Electrotechnique de Grenoble. From 2001 to 2012, he was the Manager of the Power Systems Group, Grenoble Electrical Engineering Laboratory (G2Elab), INPG. He is currently a Professor with University Grenoble Alpes. His research interests include power electronics system modelling and control, power quality, and renewable energy integration.

Mazen Alamir graduated in Mechanics (Grenoble, 1990) and Aeronautics (Toulouse, 1992). He received his Ph.D. in Nonlinear Model Predictive Control in 1995. Since 1996, he has been since a CNRS research associate in the Control Systems Department of Gipsa-lab, Grenoble. His main research topics are model predictive control, receding horizon observers, nonlinear hybrid systems, signature based diagnosis, optimal cancer treatment as well as industrial applications. He is associate editor for IEEE-TAC and served as head of the "Nonlinear Systems and Complexity" research group of the Control Systems Department of Gipsa-lab, Grenoble. Home page: www.mazenalamir.fr

Ahmad Hably received the B.S. degree in electrical engineering from the Lebanese University, Lebanon, in 2004, the M.S. degree in 2005 and the Ph.D. degree in automatic control from the Grenoble Institute of Technology, Grenoble, France, in 2007. After one year as a Researcher (ATER) with the LIRMM Laboratory, he joined the University Grenoble Alpes, Grenoble, France, as an Associate Professor at the Automatic Control Department of Grenoble Image Parole Signal Automatique Laboratory (GIPSA-lab). His research interests include electrical vehicle integration, nonlinear control, predictive control for energy systems, and airborne wind energy systems.

Cédric Boudinet was born in 1981. He graduated as an engineer in Energetic Engineering from Rouen National Institute of Applied Sciences in 2004. From 2004 to 2010, he worked as a consultant in software development for automotive, nuclear and electrical grid industries. Since 2010, he is working as an engineer in Grenoble Electrical Engineering Laboratory (G2Elab). He focuses on real-time hardware and software system.